RSC Advances

ROYAL SOCIETY OF CHEMISTRY

www.rsc.org/advances

ARTICLE TYPE www. rsc.org/xxxxxx | XXXXXXXX

Perfect Rectifying Behavior Induced by AA-P_2 Dapants in Armchair Silicene Nanoribbon Device†

Caiping Cheng,[a,b,c] **Huifang Hu,**[*b,c] **Zhaojin Zhang,**[b,c] **Haibo Zhang,**[d]

Received Xth XXXXXXXXXX 20XX, Accepted Xth XXXXXXXXX 20XX
First published on the web Xth XXXXXXXXXX 200X
DOI: 10.1039/b000000x

The band structures and electronic transport properties of AA-P_2-doped armchair silicene nanorribons (ASiNRs), introducing double phosphorus atoms into the adjacent silicon atoms at the same sublattice A, were investigated applying the density-function theory in combination with nonequilibrium Green's functions method. The results proved that the adjustment of location for AA-P_2 dopants in 7-ASiNRs obtained the semiconducting and metallic characteristics of systems. The low-bias negative differential resistance behaviors appeared symmetrically in AA-P_2-doped ASiNR devices. However, The symmetry of negative differential resistance behaviors was gradually decline with doping AA-P_2 from the center to edge. In addition, the striking rectifying behavior can be found. These outstanding properties indicated the potential application of SiNRs in nanodevice.

1 INTRODUCTION

Since stable two-dimensional (2D) graphene monolayer was first fabricated in 2004, it has become the research focus due to the high electron mobility, resulting from the Dirac cones in energy band structures.[1,2] This outstanding characteristic motivated enough enthusiasm to explore the graphene-like nanostructures. In terms of graphene itself, especially graphene nanoribbon (GNR), their electronic properties need be modulated by a controllable approach in the process of practical application. Deliberately introducing defects and impurities was an effective way to change the electronic properties. A broad range of experimental and theoretical researches reported that boron (B) and nitrogen (N) as the first choice doping elements behave like an n-type and p-type dopants in GNRs resulting in modification of electronic strutures[3–8].

Recently, a silicon analogue of graphene, named silicene, attracted extensive attention. The epitaxial single-layer silicene sheets were successfully synthesized on Ag,[9] ZrB_2,[10] Au and Ir surfaces.[11,12] This breakthrough has realized the connection between monolayer 2D nanostructures with traditional silicon technology. Silicene, unlike graphene, was a low-buckled honeycomb lattice, which attribute to a behavior in between sp^2 and sp^3 hybridization.[13] Therefore, the silicene not only had the similar electronic properties as graphene, but also showed some more superior characteristics than graphene, such as a large spin-orbit interaction,[14] quantum spin Hall effect,[15] a valley-polarized metallic phase,[16] a mechanically tunable band gap,[17–19] and so on. Using the first principles method, band structure calculations indicated the silicene was a semimetallic nano-material with zero bandgap at the Fermi level.[20–23] Therefore, a mass of studies on silicene were devoted to the open of energy bandgap. the synthesis of quasi-one-dimensional silicene nanoribbon(SiNRs) effectively has broken the bottleneck. Experimentally, the SiNRs with the width of 1.6 nm and the length of a few hundred nm has been synthesised on Ag(110) surface.[24,25] And the theoretical calculation has also demonstrated that there are two types of SiNRs, zigzag-edged SiNRs (ZSiNRs) and armchiar-edged SiNRs (ASiNRs). The ZSiNRs were always metallicity without being limited by the ribbon width, while ASiNRs exhibited metals and semiconductors depending on different ribbon widths.[26,27] The synthesis of SiNRs opened up a new opportunity for field effect transistors,[28,29] photoluminescence detector,[30] and spintronics devices et al.[31]

Different from GNR, not only B and N can insert into Si crystal lattice, but also aluminum (Al), phosphorus (P) and sulfur (S) elements can easier incorporate into SiNR.[32,33] Sivek's group studied the effect of impurities (containing B, N Al and P dopants) on the structural, electronic, and magnetic properties of silicene, which suggented that B, N, and P atoms behave like acceptors and the Al atom as donor for silicene.[34] Moreover, the effect of the B/N pair doping on the electronic properties of SiNRs was investigated by Zhang et al, and the results revealed that B/N pair can adjust the bandgap by tuning B/N pair doping site in ASiNR.[35] However, regarding P pair doping in SiNRs, no literature has been published.

[a] *College of Arts and Science, Shanxi Agricultural University, Jinzhong, 030801, P.R.China.*
[b] *School of Physics and Microelectronic Science, Hunan University, Changsha, 410082, P.R.China.*
[c] *Key Laboratory for Micro-Nano Physics and Technology of Hunan Province, Changsha, 410082, P.R.China.*
[d] *College of Environmental Science and Engineering, Hunan University, Changsha, 410082, P.R.China.*

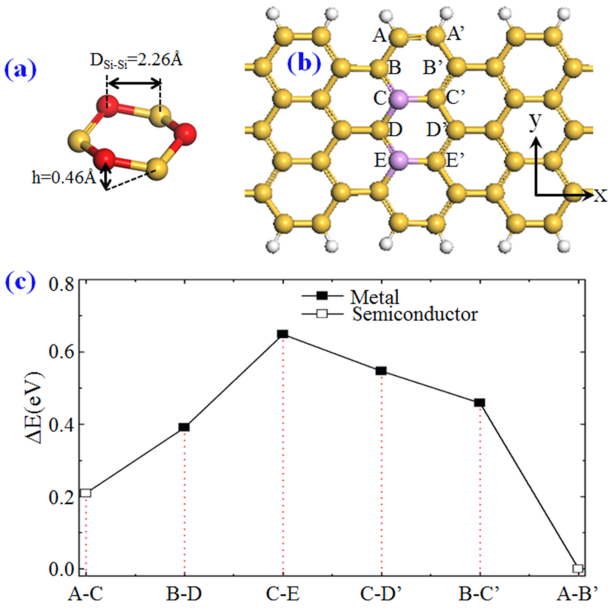

Fig. 1 (a) Structural parameters for silicene. The red atoms denote the same superlattice. (b) The schematics illustration of the surpercell of C-E configuration. The labeled capital letters stand for different doping sites to form different types of AA-P_2 dopants. Golden, white, and lilac atoms indicate silicon, hydrogen, and phosphorus atoms, respectively. (c) The relationship of total energy for AA-P_2-doped 7-ASiNRs, and all the total energy has subtracted the lowest total energy of the A-B' configuration.

In the present work, we predicted a reasonable way to tuning electronic and transport properties of SiNRs by doping two P atoms into the same silicene superlattice, which was remarked as red atom in Fig. 1(a), defined as AA-P_2. ASiNRs achieved the transition between metal and semiconductor by changing the location of AA-P_2. And we observed low-bias negative differential resistance (NDR) and striking rectifying behaviors in AA-P_2-doped ASiNRs.

2 MODELS and Methods

In this paper, the electronic band structures and transport properties were investigated for AA-P_2-doped ASiNRs, adopting the density functional theory (DFT) combined with the non-equilibrium Green function(NEGF) method. After a test calculation, we only considered the ASiNRs as a object of study, due to the location of AA-P_2 doping had no effect on the metallicity of ZSiNR. As everyone knows, each superlattice contains two different lattice structure, as positions of red and brown atoms in Fig. 1(a), which were defined as "A" and "B". On the basis of the location and direction of AA-P_2, we mainly considered two different models, (I) AA-$P_2\perp$ASiNRs, the models showed that two P atoms perpendiculared to armchair line inserted to the same superlattice "A" of ASiNRs, and were marked as A-C, B-D , C-E from edge to center. (II) AA-$P_2\angle$ASiNRs, the models showed that two P atoms perpendicular to diagonal armchair line inserted to the same superlattice "A"of ASiNRs, and were marked as C-D, B-C, A-B from center to edge. Fig. 1(b) show the diagram of C-E constructions based on ASiNRs, in which two P atoms substituted silicon atoms labeled by capital letters and formed AA-P_2-doped ASiNRs in a super cell consisted of three unit cell. The edge silicon atoms were inactivated by hydrogen. Compared with GNRs, the study found that the band gap of SiNRs also depended on the width of ribbon, while GNRs had larger band gaps than SiNRs with the same ribbon width. So, bandgap variation for SiNR was separated into three types namely N=3n +1, 3n and 3n-1, with n integer.[36] In addition, the bandgap decreases along with the increase of nanoribbons width, resulting from the quantum confinement effect (QCE).[37,38] Trivedi et al. proved that the 3n +1 type of SiNRs has large band gaps compared to 3n and 3n-1.[39] Therefore, we chose the width of AA-P_2-doped ASiNRs with seven dimer lines (N=7).

The geometric structure optimization and ectronic band structures calculation was performed in the Spanish Initiative for Electronic Simulations with Thousands of Atoms (SIESTA) package.[40,41] The generalized gradient approximation (GGA) parameterized by Perdew Burke Ernzerhof (PBE) were adopted for the exchange-correlation potential.[42] To achieve the balance between calculation accuracy and flexibility, the fully structural optimizations were carried out by $10\times1\times1$ Monkhorst-Pack k points sampling until the residual forces on the atoms were less than 0.02eV/Å^{-1} and the difference in total energy was less than 10^{-5}eV. In the self-consistent total-energy calculations, the Brillouin zone (BZ) was sampled by $23\times1\times1$ Monkhorst-Pack k points. The cutoff energy was set to 200Ry. The atomic orbital basis set was the double-ζ plus polarization (DZP) basis set.

The transport properties calculations were performed by TRANSIESTA-C package.[40,41,43] The standard equation about voltage transmission spectrum:

$$T(E, V)=\mathrm{Tr}[\Gamma_L(E, V)G(E, V)\Gamma_R G^{\dagger}(E, V)$$

where G was the Greens function of the contact region, $\Gamma_{L/R}$ was the coupling matrix, and V was the applied voltage bias. The computational formula of current can be used namely, the Landauer-Büttiker formula:

$$I=2e/h\int_{-\infty}^{+\infty}dE[f_L(E-\mu_L)-f_R(E-\mu_R)]T(E, V)$$

where μ_L and μ_R were the electrochemical potentials for the two electrodes and T (E, V) was the transmission coefficient at energy E and bias voltage V.[43]

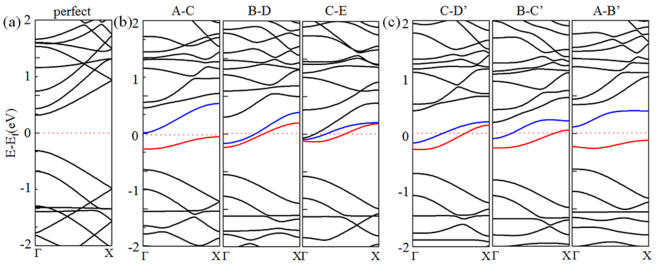

Fig. 2 (a)-(c) Band structure of pristine 7-ASiNR, AA-P_2 vertical doping ASiNRs, AA-P_2 diagonal doping ASiNRs, repectively. The Fermi level is set to zero, remarked as the red dotted line. The red and blue bands stand for the impurity subbands from AA-P_2 dopants in 7-ASiNRs.

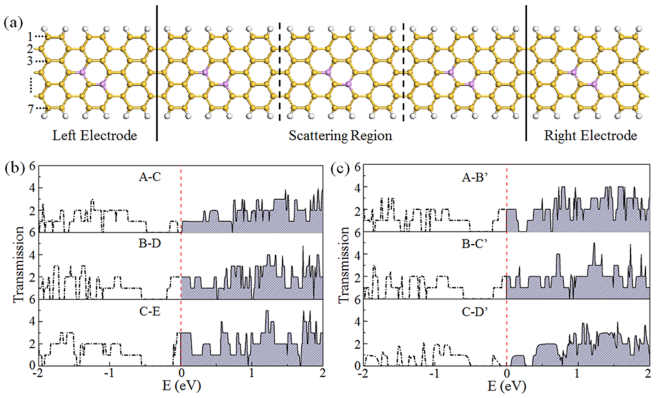

Fig. 3 (a) The schematic of two-probe transport model of D-E' configuration. The lilac atoms standed for the position of phosphorus atoms. Numbers at left side indicate the width of ASiNRs. (b)-(c) The transmission spectra of AA-P_2 vertical doping ASiNRs and AA-P_2 diagonal doping ASiNRs at the equilibrium state, respectively. The dot-dash line and shadow parts denote the transmission spectra at the positive and negative energies.

3 Result and discussion

Unlike the planar graphene sheets, the stable structure of silicene sheet was buckled as shown in Fig.1(a), and we can predict higher surface activity due to sp^2 and sp^3 mixed hybrid lattice structure. After the structure optimization, The Si-Si bond lengths varied from 2.26Å at the edge to 2.28Å at the center and the Si-H bond length was about 1.51Å. The calculated total energy of AA-P_2-doped ASiNRs systems presented in Fig.1(c) and has subtracted the lowest total energy in A-B' system (-734.5eV). The results clearly showed that A-B' configuration was the most stable structure. the difference of negative total energies in these AA-P_2-doped systems is small, which implies that the AA-P_2-doped systems are all relatively stable. Obviously, in Fig1(c), the configurations of A-C and A-B were more favorable energetically than others, suggesting that the AA-P_2 style was more likely to incorporate at the edge of nanoribbons. Considering the P atoms incorporated at the edge of A-C system, the lengths of Si-H and P-Si bonds were 1.46 Å and 2.25 Å, respectively, and it was shorter than the edge Si-H and Si-Si bonds 1.51Å and 2.26 Å, leading to a slight local deformation in the system. Moreover, when the exotic P atoms gradually closed to the center, the bond lengths between the P-Si atoms also slightly shorter than the initial Si-Si bond (2.26 Å), which demonstrates a stronger interaction between P and Si atoms.

The electronic band structures of AA-P_2-doped ASiNRs were investigated using periodic boundary condition and plotted in Figs.2(a)-2(c), corresponding to pristine 7-ASiNR, AA-P_2⊥ASiNRs and AA-P_2∠ASiNRs systems, respectively. The perfect 7-ASiNR exhibited typical semiconducting characteristic with a band gap of 0.52 eV between π and π^* bands at Γ point in Fig.2(a), which was consistent with 0.57eV reported by Trivedi et al.[39] Similar to GNRs, impurity atoms in SiNRs also obvously changed the site of bands in Fig.2(b) and 2(c). We found that inserted AA-P_2 caused a shift of Fermi level (E_F) into conduction bands and made overall bands moved down, which suggested that two extra electrons of AA-P_2 formed the local states within the region of the conduction bands. On the other hand, the introducing of AA-P_2 impurity not only changed the site of bands, but also can modulate the bandgap of SiNRs. As inserting AA-P_2 into ASiNRs, P atoms generated two new impurity subbands between π and π^* bands, which indicated that P atoms played the role of the donors. As for AA-P_2⊥ASiNR systems in Fig.2(b), AA-P_2 dopants provided extra two electrons for ASiNRs and the band gaps obviously decreased along with the location of AA-P_2 from edge to center. For example, A-C system remained a bad gap about 0.08eV. However, for B-D and C-E system, two new subbands touched each other and intersected with E_F, so that the bandgap disappeared and displays typical metallic feature. More interesting was that impurity states in the vicinity of E_F was more delocalized with the location of P atoms from edge to center. Moreover, for AA-P_2∠ASiNR systems, as introducing AA-P_2 dopants from center to edge of nanoribbon, two subbands were so slightly separated until completely displayed a bandgap about 0.21eV in A-B' configuration. As a result, by changing the location of AA-P_2 in the 7-ASiNRs, the semiconducting and metallic characteristics of systems can be obtained. As far as we known, this location-dependent electronic property observed here was reasonable agreement with related theories about graphene nanoribbons.[44,45]

To investigate the effect of AA-P_2 on the electronic transport property in 7-ASiNRs, we calculated the electronic transport properties. First of all, we exhibited the two-probe transport model of AA-P_2-doped ASiNR devices, as shown in Fig.3(a) typified by D-E' configuration, as shown in Fig.3(a). The two-probe model consisted of left lead, scattering cen-

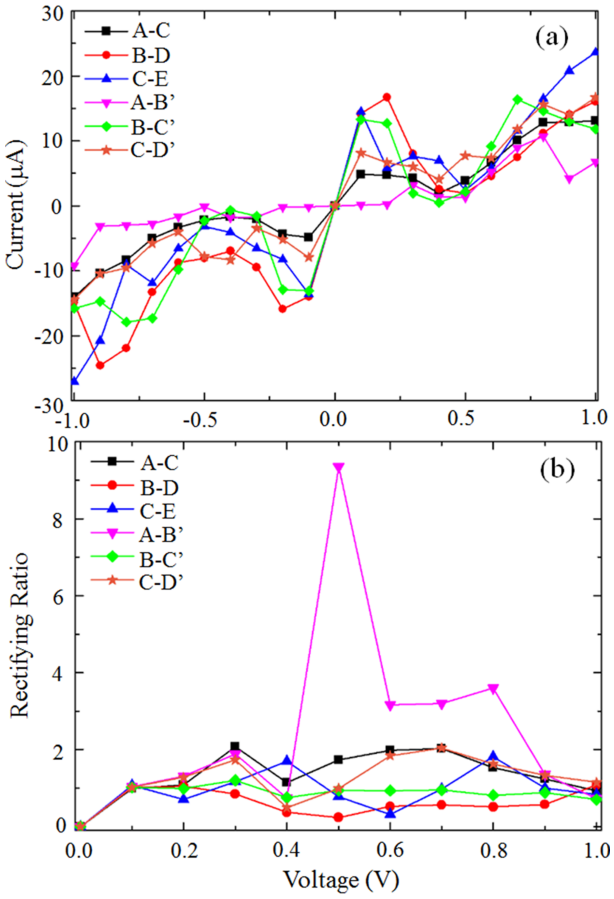

Fig. 4 (a) Current-voltage (I-V) characteristics of AA-P_2-doped ASiNR devices with the bias voltage varying from -1.0V to 1.0V in a step of 0.1 V. (b) Rectification ratio as a function of the bias for AA-P_2-doped ASiNR devices from 0.1V to 1.0V.

ter region and right electrode, respectively. The scattering center region linked up with half-infinite AA-P_2-doped ASiNR electrodes and contained three super cells, each of which was combination with three sequential silicon unit cell. The transmission spectra of AA-P_2⊥ASiNRs and AA-P_2∠ASiNRs systems at the equilibrium state were plotted in Fig.3(b) and 3(c). The conducting channels of systems were promoeted by introducing impurity bands, the small transmission gaps appeared at the E_F of A-C and C-D' systems compared with perfect 7-ASiNR. About $2G_0$ ($G_0=2e^2/h$) transmission peaks from the flat near the E_F appeared in A-B', B-D and B-C', which showed the visible metallic character. In particular, the peak about $3G_0$ appeared at the E_F of C-E configuration in accordance with the electronic band structure of C-E. So, we reached a conclusion that changing the sites of P atoms significantly altered the zero-bias transport properties with semiconducting and metallic characteristics in AA-P_2-doped ASiNR.

In order to evaluate the transition between metal and semiconductor, and deeply explore the transport properties by changing the location of AA-P_2 in 7-ASiNRs, the current-voltage (I-V) characteristic curve of all AA-P_2-doped ASiNR devices were presented in Fig.4(a) at the bias range from -1 to +1V in steps of 0.1 V. The current of all devices increase rapidly to reach peak values first, then currents decreased and fell to the lowest with the increases of the bias, appearing the nice NDR behavior. As to AA-P_2⊥ASiNR systems, the magnitude of current in A-C device was significantly less than B-D and C-E systems. Similarly, as for AA-P_2∠ASiNRs, not only the current decreased but also the symmetry of current was destroyed under the positive and negative voltage. On this basis, we can draw a conclusion that the NDR behaviors of AA-P_2-doped ASiNR devices depended on the location of AA-P_2 and the symmetry of geometric structure was broken by the edge of doping to weaken the conduction ability. Furthermore, it is interesting that NDR effect generally appeared within high bias regions, while NDR behaviors in our devices can be observed at so low bias (from 0.0 to 0.4V), which reduced power consumption in the devices design process. Although the edge doping of AA-P_2 reduced the current for A-B' system and weaken the NDR behavior, the rectifying behaviors still can be observed. According to the basic definition of rectifying ratio, R(V)=I(V)/I(-V), we plotted the rectifying ratio curves on AA-P_2-doped ASiNRs in Fig.4(b). From the figure, we can see that the rectifying ratio of B-D and B-C' systems was almost 1 within the scope of the calculated bias. It means that the magnitude of opposite current were almost the same on the positive and negative bias. Howerer, A-B' device appeared the biggest rectifying ratio about 10 at 0.5V. When the symmetrical structure of system was broken, the magnitude of current decreases leading to the current of A-B' was smaller than others. The NDR behaviors still existed, however, the peak-to-valley ratio (PVR) on positive bias region is

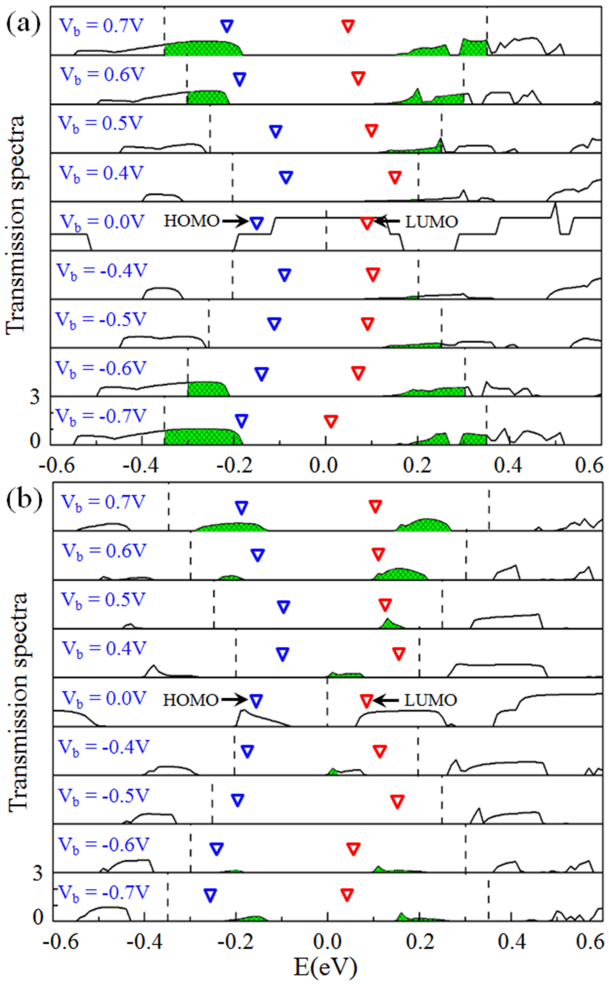

Fig. 5 (a)-(b) Bias-dependent transmissions of B-C' and A-B' configurations from ±0.4V to ±0.7V in step of 0.1 V. The dashed lines are bias window and the green part denotes the real integral area of the bias window. The red and blue triangles stand for HOMO and LUMO, respectively.

larger than that on negative bias region to perform a rectifying behavior. These outstanding behaviors indicated potential application of AA-P_2-doped ASiNRs in nanomaterials-based devices.

To explain the strong rectification behavior, the bias-based transmission spectra was plotted in Fig.5. As we known, the current was determined by the integral region in the bias windows from the Landauer-Büttiker formula. Furthermore, the interaction between the highest occupied molecular orbital (HOMO) and lowest unoccupied molecular orbital (LUMO) was one of important factors to influence the conductivity of systems. In other words, the smaller the distance between the two orbitals were, the stronger the conductance ability. For the B-C' configuration in Fig.5(a), the real integral areas were almost the same at biases with identical absolute value, such as ±0.4, ±0.5, ±0.6 and ±0.7V. The gap between HOMO and LUMO was nearly invariable at the equal absolute voltage values so that the rectifying ratio maintain 1. As to the A-B' in Fig.5(b), however, the integral areas and two orbitals was no longer symmetric at the same bias absolute value leading to appear the rectify behavior, which the biggest ratio was almost as much as 10 at 0.5V. We can see the obvious transferring channels in the bias window at 0.5V, while the transmission coefficients were almost zero in the bias window at -0.5V. On the other hand, the gap between HOMO and LUMO at 0.5V was more closer than -0.5V. In consequence, A-B' device appeared prominent rectifying behavior. The reason for this phenomenon is rooted in the doped effect of phosphorus atoms. It is well known that a phosphorus atom has one more electron than a silicon atom. When two silicon atoms at the same sublattice A were replaced by AA-P_2 in A-B' system, the additional electrons was injected to the system and the Fermi energy was pushed up slightly. In addition, the doping of phosphorus atoms was only performed on one side of ASiNRs which made the distributing of electrons different on two system sides. So, the A-B' showed a rectifying behavior like a p-n junction which was consistent with the previous rectifying mechanism.[46–48] We can predict that the unique electronic transport properties of the ASiNRs incorporated to AA-P_2 dopants could be very useful for designing silicene-based molecular devices.

4 Conclusions

The bandgap variation and transport properties of AA-P_2-doped 7-ASiNR devices were investigated applying DFT theory combined with NEGF method. Compared with the total energy between different types of AA-P_2-doped ASiNRs, the results made clear that the configurations with AA-P_2 situating on the edge of ASiNRs, such as A-C and A-B', were the most stable. The interesting thing was that the semiconducting and metallic characteristics had been observed by changing the doping location of AA-P_2 in 7-ASiNRs. In addition, the different location of P atoms inserted into ASiNR will disrupt the distribution of electrons resulting in the symmetric NDR and obvious rectifying behavior at low-bias region. In especial, the rectifying ratio of A-B' configuration can reach up to 10 at 0.5V. So, we predict that a way by adjudting the position of AA-P_2 dopants in ASiNR could realize the transition between semiconductor with metal, which provided a theoretical basis for the design of silicene-based electronic devices.

Acknowledgments

This work was supported by the National Basic Research (973) Program of China (Grant No. 2011CB932700), and the Aid Program for Science and Technology Innovative Research Team in Higher Educational Institutions of Hunan Province.

References

1 K. S. Novoselov, A. K. Geim, S. V. Morozov, D. Jiang, Y. Zhang, S. V. Dubonos, I. V. Grigorieva and A. A. Firsov, *Science*, 2004, **306**, 666.
2 A. K. Geim and K. S. Novoselov, *Nat. Mater.*, 2007, **6**, 183.
3 Z. Sheng, H. Gao, W. Bao, F. Wang and X. Xia, *J. Mater. Chem.*, 2012, **22**, 390.
4 Y. Wang, Y. Shao, D. Matson, J. Li and Y. Lin, *ACS Nano.*, 2010, **4**, 1790.
5 T. B. Martins, R. H. Miwa, A. J. R. da Silva and A. Fazzio, *Plys. Rev. Lett.*, 2007, **98**, 196803.
6 P. Marconcini, A. Cresti, F. Triozon, G. Fiori, B. Biel, Y. Niquet, M. Macucci and S. Roche, *ACS Nano.*, 2012, **6**, 7942.
7 W. Yao, K. Yao, G. Gao, H. Fu and S. Zhu, *Solid State Commun.*, 2013, **153**, 46.
8 J. Zeng, K. Q. Chen, J. He, Z. Q. Fan and X. J. Zhang, *J. Appl. Phys.*, 2011, **109**, 124502.
9 P. Vogt, P. D. Padova, C. Quaresima, J. Avila, E. Frantzeskakis, M. C. Asensio, A. Resta, B. Ealet and G. L. Lay, *Phys. Rev. Lett.*, 2012, **108**, 155501.
10 A. Fleurence, R. Friedlein, T. Ozaki, H. Kawai, Y. Wang and Y. Yamada-Takamura, *Phys. Rev. Lett.*, 2012, **108**, 245501.
11 M. R. Tchalala, H. Enriquez, A. J. Mayne, A. Kara, S. Roth, M. G. Silly, A. Bendounan, F. Sirotti, T. Greber and B. Aufray, *Appl. Phys. Lett.*, 2013, **102**, 083107.
12 L. Meng, Y. Wang, L. Zhang, S. Du, R. Wu, L. Li, Y. Zhang, G. Li, H. Zhou and W. A. Hofer, *Nano. Lett.*, 2013, **13**, 685.
13 E. Cinquanta, E. Scalise, D. Chiappe, C. Grazianetti, B. van den Broek, M. Houssa, M. Fanciulli and A. Molle, *J. Phys. Chem. C*, 2013, **117**, 16719.
14 C. C. Liu, H. Jiang and Y. Yao, *Phys. Rev. B*, 2011, **84**, 195430.
15 C. C. Liu, W. Feng and Y. Yao, *Phys. Rev. Lett.*, 2011, **107**, 076802.
16 M. Ezawa, *Phys. Rev. Lett.*, 2012, **109**, 055502.
17 Z. Ni, Q. Liu, K. Tang, J. Zheng, J. Zhou, R. Qin, Z. Gao, D. Yu and J. Lu, *Nano. Lett.*, 2012, **12**, 113.
18 S. Huang, W. Kang and L. Yang, *Appl. Phys. Lett.*, 2013, **102**, 133106.
19 M. Topsakal and S. Ciraci, *Phys. Rev. B*, 2010, **81**, 024107.
20 K. Takeda and K. Shiraishi, *Phys. Rev. B*, 1994, **50**, 14916.
21 S. Cahangirov, M. Topsakal, E. Akturk, H. Sahin and S. Ciraci, *Phys. Rev. Lett.*, 2009, **102**, 236804.
22 G. G. Guzman-Verri and L. C. L. Y. Voon, *Phys. Rev. B*, 2007, **76**, 075131.
23 L. Chen, C. C. Liu, B. Feng, X. He, P. Cheng, Z. Ding, S. Meng, Y. Yao and K. Wu, *Phys. Rev. Lett.*, 2012, **109**, 056804.
24 P. Padova, C. Quaresima, C. Ottaviani, P. M. Sheverdyaeva, P. Moras, C. Carbone, D. Topwal, B. Olivieri, A. Kara, H. Oughaddou, B. Aufray and G. L. Lay, *Appl. Phys. Lett.*, 2010, **96**, 261905.
25 B. Aufray, A. Kara, S. Vizzini, H. Oughaddou, C. Landri, B. Ealet and G. L. Lay, *Appl. Phys. Lett.*, 2010, **96**, 183102.
26 S. Cahangirov, M. Topsakal and S. Ciraci, *Phys. Rev. B*, 2010, **81**, 195120.
27 Y. Song, Y. Zhang, J. Zhang and D. Lu, *Appl. Surf. Sci.*, 2010, **256**, 6313.
28 H. Li, L. Wang, Q. Liu, J. Zheng, W. Mei, Z. G. abd J.J. Shi and J. Lu, *Eur. Phys. J. B*, 2012, **85**, 274.
29 N. D. Drummond, V. Zlyomi and V. I. Falko, *Phys. Rev. B*, 2012, **85**, 075423.
30 F. Xia, T. Mueller, Y. Li, A. Valdes-Garcia and P. Avouris, *Nat. Nanotechnol.*, 2009, **4**, 839.
31 T. C. H. L. H. J. W.F. Tsai, C. Huang and A. Bansil, *Nat. Commun.*, 2013, **4**, 1500.
32 F. Zheng, C. Zhang, S. Yan and F. Li, *J. Mater. Chem. C*, 2013, **1**, 2735.
33 R. Wang, M. Xu and X. Pi, *Chin. Phys. B*, 2015, **24**, 086807.
34 J. Sivek, H. Sahin, B. Partoens and F. M. Peeters, *Phys. Rev. B*, 2013, **87**, 085444.
35 H. Luan, C. Zhang, F. Zheng and P. Wang, *J. Phys. Chem. C*, 2013, **117**, 13620.
36 L. Ma, J. Zhang, K. Xu and V. Ji, *Physica B*, 2013, **425**, 66.
37 U. Treske, F. Ortmann, B. Oetzel, K. Hannewald and F. Bechstedt, *Phys. Status Solidi A*, 2010, **207**, 304.
38 A. Srivastava, A. Jain, R. Kurchania and N. Tyagi, *J. Comput. Theor. Nanosci.*, 2012, **9**, 1008.
39 S. Trivedi, A. Srivastava, R. Kurchania and J. Comput, *Theor. Nanosci.*, 2014, **11**, 789.
40 M. S. Jose, A. Emilio, D. G. Julian, G. Alberto, J. Javier, O. Pablo and S. P. Daniel, *J. Phys. Condensed Matt.*, 2002, **14**, 2745.
41 P. Ordejon, E. Artacho and J. M. Soler, *Phys. Rev. B*, 1996, **53**, R10441(R).
42 J. P. Perdew, K. Burke and M. Ernzerhof, *Phys. Rev. Lett.*, 1996, **77**, 3865.
43 M. Brandbyge, J. L. Mozos, P. Ordejn, J. Taylor and K. Stokbro, *Phys. Rev. B*, 2002, **65**, 165401.
44 T. Chen, X. Li, L. Wang, Q. Li, K. Luo, X. Zhang and L. Xu, *J. Appl. Phys.*, 2014, **115**, 053707.
45 N. Xu, B.L.Wang, D. Shi and C. Zhang, *Solid State Commun.*, 2012, **152**, 994.
46 D. H. Zhang, K. L. Yao and G. Y. Gao, *J. Appl. Phys.*, 2011, **110**, 013718.
47 X. H. Zheng, X. L. Wang, Z. X. Dai and Z. Zeng, *J. Chem. Phys.*, 2011, **134**, 044708.
48 X.-Q. D. G.-P. T. Zhi-Qiang Fan, Zhen-Hua Zhang and K.-Q. Chen, *Appl. Phys. Lett.*, 2013, **102**, 023508.